

Model for the director and electric field in liquid crystal cells having twist walls or disclination lines

G. Panasyuk^{a)} and D. W. Allender

Liquid Crystal Institute and Department of Physics, Kent State University, Kent, Ohio 44242

(Received 27 December 2001; accepted for publication 20 March 2002)

Two examples of the director structure and electric field in patterned electrode liquid crystal cells are studied using a recently developed calculational model. First, a display cell that exhibits a homeotropic to multidomainlike transition with twist wall structures has been considered for a liquid crystal with positive dielectric anisotropy. The model elucidates the behavior of the electric field. Calculations show good agreement between the model and direct computer solution of the Euler–Lagrange equations, but the model is at least 30 times faster. Second, the possibility that a cell has $\pm 1/2$ disclination lines instead of a wall defect is probed. A temperature dependent estimate for the size of the defect core is given, and the total free energy of the cell with disclination lines was calculated and compared with the corresponding value for the same cell with wall defect structure.

© 2002 American Institute of Physics. [DOI: 10.1063/1.1477613]

I. INTRODUCTION

For the last several years liquid crystal displays (LCDs) have become increasingly used in laptop computers, TVs and monitors. The image quality and the resolution of LCDs have been improved. Most of the newly developed LCDs, with wide viewing angle, good color characteristics and fast response time, possess a multidimensional director distribution which means that the director \mathbf{n} depends on two or three space coordinates unlike in the case of twisted nematic displays. Among these new devices are a LCD which combines the concept of in-plane switching (IPS) with vertical alignment (VA),^{1–5} a display associated with a homeotropic to multidomainlike (HMD) transition,^{6,7} fringe-field switching devices,^{8,9} and a liquid crystal (LC) π cell with patterned electrodes.¹⁰ As LCDs become more sophisticated, accurate and effective LCD modeling methods are becoming increasingly important.

In earlier publications^{4,5} a model was developed to describe properties of LC cells with wall defect layers where \mathbf{n} lies in one plane and there is no twist deformation (see Fig. 1). The purpose of this work is, first of all, to generalize the model to describe a LC cell with a twist wall and, second, to modify the model to include the possibility of cells with $\pm 1/2$ disclination lines.

An example of a LC cell with twist wall defects is a HMD display (see Fig. 2). It has a three-dimensional (3D) director \mathbf{n} and electric field \mathbf{E} . The electrodes and surface coating of the HMD display are prepared in such a way that in the absence of \mathbf{E} the LC alignment for a nematogen with positive dielectric anisotropy ϵ_a is homeotropic. Strong homeotropic anchoring occurs at the cell substrates. In Sec. II a model is developed to describe \mathbf{n} and \mathbf{E} for the HMD mode for voltage differences, u , that are high enough that the transmittance of light is observable. In Sec. III a simplified but still accurate way of calculating the LC alignment of a cell

with $\pm 1/2$ disclination lines and its free energy will be described.

II. MODELING OF THE HMD LC CELL

As was shown in Ref. 7, the HMD LC cell possesses the following symmetries: (1) $2L$ periodicity along both the x and y directions for any variables; (2) mirror symmetry with respect to the vertical planes at $x = \pm L/2, \pm 3L/2, \dots$, and $y = \pm L/2, \pm 3L/2, \dots$; (3) “twisted symmetry,” where, for example, $\Phi(x, y, z) = \Phi(y, x, -z)$, and (4) electric potential that satisfies the relation $\Phi(x, y, z) = -\Phi(-x, -y, z)$. Due to these symmetries, it is enough to consider only the volume inside the right triangle prism with the triangle ΔOAB as its horizontal cross section (see Fig. 2) and then extend the results of calculation of the director and electric field to the rest of the cell using symmetry. As has already been noted,⁷ two different defect structures are conceivable for the director configuration: one with a system of wall defects and the other with disclination lines. For small voltages u , a simple estimate⁷ indicates the configuration with wall defects will occur. Also, the results of light transmittance measurements⁶ have been interpreted in terms of a system of wall defects, at least for the most interesting range of display voltages, $u \leq 20$ V. Thus, for the HMD cell the director configuration

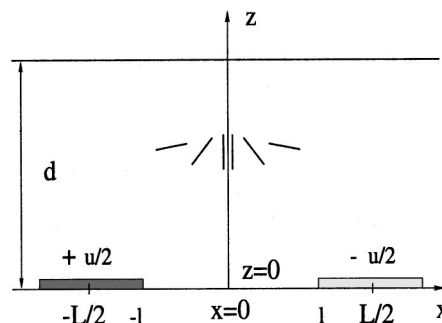


FIG. 1. Schematic diagram of the 2D cell.

^{a)}Electronic mail: georgy@columbo.kent.edu

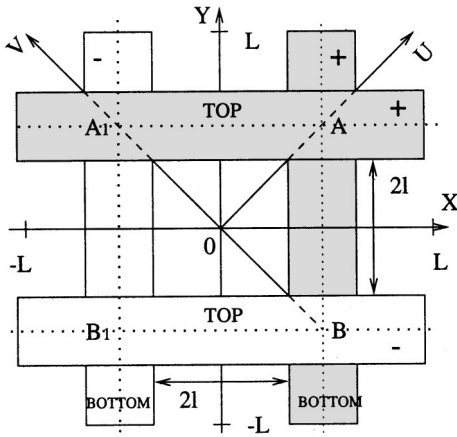


FIG. 2. Top view of the HMD cell. The electrode planes have coordinates of $z = \pm d/2$. Planes of mirror symmetry are shown as dotted lines.

with wall defects is the most important to consider. Wall defect layers lie approximately along vertical diagonal planes like the UZ plane in Fig. 2 which is the center plane of the defect. Along these wall defect layers \mathbf{E} is approximately perpendicular to director \mathbf{n} , the torque due to the electric field is close to zero and the director remains close to homeotropic even in the presence of \mathbf{E} .

Taking into account these symmetries, the total free energy of the system can be written as

$$F = \int d\rho \int_{-d/2}^{d/2} dz (f_d + f_e) - \frac{\epsilon_g}{8\pi} \times \int d\rho \left(\int_{-\infty}^{-d/2} + \int_{d/2}^{\infty} \right) dz E^2, \quad (1)$$

where

$$f_d = \frac{K_1}{2} (\nabla \cdot \mathbf{n})^2 + \frac{K_2}{2} [\mathbf{n} \cdot (\nabla \times \mathbf{n})]^2 + \frac{K_3}{2} [\mathbf{n} \times (\nabla \times \mathbf{n})]^2, \quad (2)$$

and

$$f_e = -\frac{\epsilon_a}{8\pi} (\mathbf{n} \cdot \mathbf{E})^2 - \frac{\epsilon_{\perp}}{8\pi} E^2, \quad \epsilon_a = \epsilon_{\parallel} - \epsilon_{\perp} > 0. \quad (3)$$

Due to symmetry, the integration over ρ in the horizontal plane can be restricted to triangle ΔOAB .

The main idea of the proposed model⁴ is to numerically solve the dynamic equation¹¹

$$\gamma_1 \partial_t \mathbf{n} = -\delta \mathbf{F} / \delta \mathbf{n} \quad (4)$$

using the exact expression for the free energy but an approximate expression for the electric field \mathbf{E} found in this work. Here γ_1 is the rotational viscosity and flow is neglected. In contrast, previously used methods of direct computer calculation (see, for example, Refs. 12–14) do not use an approximate form for the electric field but instead solve $\nabla \cdot \mathbf{D} = 0$ to get the electric field after each director update, based on Eq. (4).

A. Approximation of the electric field

To find a reasonable approximation for \mathbf{E} , let us introduce high voltage $\mathbf{E}^h = -\nabla \Phi^h$ and low voltage $\mathbf{E}^l = -\nabla \Phi^l$ asymptotics as the solutions of the corresponding equations,

$$\nabla_{\perp}^2 \Phi^h + \partial_z^2 \Phi^h = 0, \quad (5)$$

$$\nabla_{\perp}^2 \Phi^l + (\epsilon_{\parallel} / \epsilon_{\perp}) \partial_z^2 \Phi^l = 0, \quad (6)$$

with the conditions $\Phi^{h,l}(\mathbf{r}) = \pm u/2$ on the electrodes and $\mathbf{E}^{h,l}(\mathbf{r}) \rightarrow 0$ when $|z| \rightarrow \infty$. Equation (6) is the Maxwell equation $\nabla \cdot \mathbf{D} = 0$ with $\mathbf{n} \equiv \hat{z}$ everywhere inside the cell. Here the subscript “ \perp ” for a vector means its components are in a plane perpendicular to the z axis, specifically, $\nabla_{\perp} = \hat{x} \partial_x + \hat{y} \partial_y$. The solution $\Phi^h(\mathbf{r})$ was obtained and it is described in detail in Ref. 7 [where it was denoted $\Phi_0(\mathbf{r})$]. Similar to $\Phi^h(\mathbf{r})$, the solution $\Phi^l(\mathbf{r})$ may be represented by a truncated Fourier series and can be produced from $\Phi^h(\mathbf{r})$ with the following substitutions in the Fourier coefficients [see the text between Eqs. (49) and (50) in Ref. 7]:

$$B_{pq} \rightarrow d_{pq}^1 \left[2 + \hat{\epsilon} \frac{\epsilon_{\parallel}}{\epsilon_g} (\tanh d_{pq}^1 + \coth d_{pq}^1) \right],$$

$$G_{mpq} \rightarrow \hat{\epsilon} \frac{\epsilon_{\parallel}}{2\epsilon_g} d_{pq}^1 a_{mq} (\tanh d_{pq}^1 - \coth d_{pq}^1),$$

where $\hat{\epsilon} = (\epsilon_{\perp} / \epsilon_{\parallel})^{1/2}$, $d_{pq}^1 = \pi \hat{\epsilon} d [(2p+1)^2 + 4q^2]^{1/2} / 2L$ and we took into account that the medium outside the LC slab is a uniform glass plate with a dielectric constant ϵ_g [see the text after Eq. 60 in Ref. 7]. The low voltage potential in the glass plates is determined by formula (40) in Ref. 7, but $\Phi_{LC} \equiv \Phi^l$ inside the LC film is determined from Eq. (39) in Ref. 7, where d_{pq} in this equation must be substituted by d_{pq}^1 .

As was shown before,⁷ for relatively high voltages it is possible to provide a reasonable description of the cell by dividing it into two near-substrate layers with thicknesses of $\Delta_1 \approx \Delta_2 \approx 2\xi$ [$\xi = (4\pi K_{13} / \epsilon_a)^{1/2}$ is the correlation length, where $K_{13} = (K_1 + K_3) / 2$] and a bulk region between them where $\mathbf{E} \approx \mathbf{E}^h$. On the other hand, in all the displays mentioned in Sec. I d is much less than L (usually $d/L \leq 0.2$). Thus, to estimate the influence of the substrate layers on the electric field, one can neglect ∇_{\perp} in the Euler–Lagrange equations for the director and electric field. Neglecting ∇_{\perp} in the Maxwell equation $\nabla \times \mathbf{E} = 0$ shows that one can also neglect the z derivative of \mathbf{E}_{\perp} . This means that small length scale changes in the director field near a substrate do not produce the same significant changes in \mathbf{E}_{\perp} . In such a situation $\mathbf{E}_{\perp} \approx \mathbf{E}^h$ even across a near-substrate layer.⁴ Omitting ∇_{\perp} in the Maxwell equation $\nabla \cdot \mathbf{D} = 0$, one can find E_z from

$$\nabla \cdot \mathbf{D} \approx \partial_z D_z = 0. \quad (7)$$

Thus, in the first approximation $\mathbf{E}_{\perp} \approx \mathbf{E}_{\perp}^h$, and, after integration Eq. (7), E_z can be presented as

$$E_z \approx [\epsilon_{zzm} E_{zm}^h + \epsilon_a (\mathbf{n}_{\perp m} \cdot \mathbf{E}_{\perp m}^h n_{zm} - \mathbf{n}_{\perp} \cdot \mathbf{E}_{\perp}^h n_z)] \epsilon_{zz}^{-1}, \quad (8)$$

where $\epsilon_{zz} = \epsilon_{\perp} + \epsilon_a n_z^2$ and index “ m ” means that $z=0$ must be taken in the corresponding value ($z=0$ is the midpoint between the substrates).

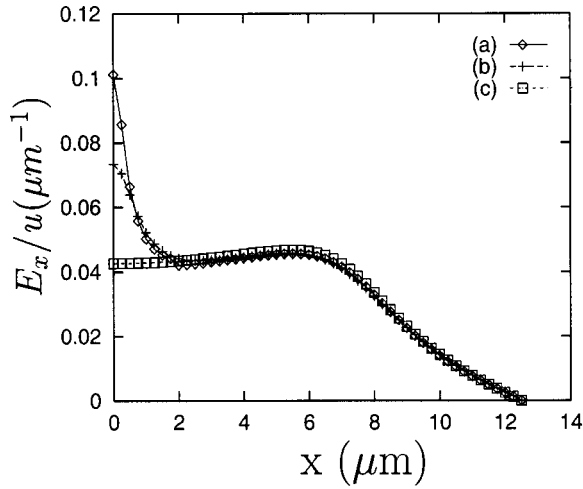


FIG. 3. $E_x(x, z=d/2)$ at $u=14$ V in the 2D cell obtained from (a) the model, (b) direct computer solution, and (c) E_x^h .

When u decreases, the bulk region shrinks and finally disappears at $u < u_0$, where u_0 can be estimated from the relation $4\xi=d$. For the experimental set of HMD cell parameters,⁶ $u_0=8$ V (dark state for this display observed⁶ for $u < 5$ V). When $u < u_0$, E_z deviates significantly from E_z^h and formula (8) fails to describe E_z properly for the important region of small $|v|$. The same arguments as those in Ref. 4 provide us with the following expression for $E_z(u, v, z)$:

$$E_z \approx (\epsilon_a / \epsilon_{||}) \mathbf{n}_{\perp} \cdot \mathbf{E}_{\perp}^h + E_z^l, \quad (9)$$

when $|v| < \delta$, where δ is the largest value of the v coordinate for which the approximate relation $\epsilon_{zz} \approx \epsilon_{||}$ is still satisfied with about 10% accuracy. The value of δ is a function of u and the other cell parameters and is found in the course of solving Eq. (4). For low voltages, when $u < u_0$, δ is relatively large (it may be comparable to $l/2$), but when u increases, δ decreases quickly and for $u \geq 10$ V, $\delta < \xi$ and Eq. (8) is applicable for all v . It is worth mentioning that formulas (8) and (9) are a direct generalization of relations (24) and (26) in Ref. 4 obtained in the course of describing the two-dimensional (2D) cell and can be produced from Eqs. (24) and (26) in Ref. 4 by substituting $n_x E_x^h \rightarrow \mathbf{n}_{\perp} \cdot \mathbf{E}_{\perp}^h$. As was shown in Refs. 4 and 5, for higher voltages, when $u > u_0$, E_x^h for the 2D cell must be also modified in the wall's defect region to take into account small length scale changes in the director field across the wall's defect layer when \mathbf{n} changes from homeotropic at the center of the defect to close to planar distribution outside. According to those director variations, the largest component E_x of the electric field which is perpendicular to the wall's defect layer, also changes significantly, having a peak in the center of the wall defect layer (see Fig. 3). On the other hand, as follows from the geometry of the HMD cell, the electric field component E_v perpendicular to the wall defect layer is negligible (unlike in the 2D case). The largest field component E_u is now along the wall-defect layer. It causes \mathbf{n} to twist in the wall layer,⁷ but E_u itself does not show any peculiarities inside the layer in Fig. 4. This means that one can neglect the influence of the wall defect

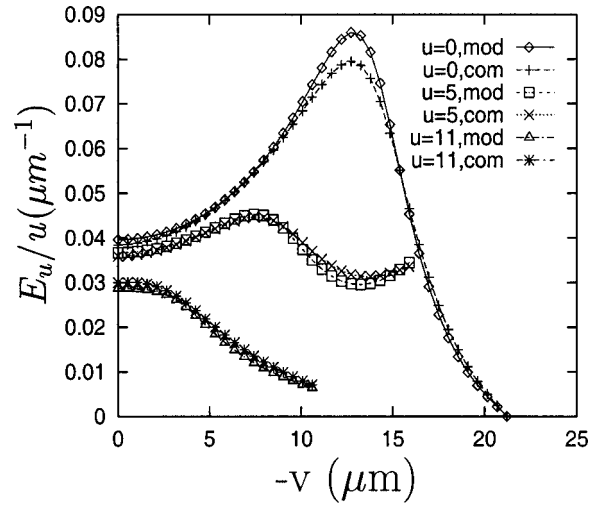


FIG. 4. E_u dependence on the v coordinate at 14 V in the HMD cell calculated by the model and direct computer calculation for different values of the u coordinate (in μm).

layer on \mathbf{E} in this case of the twist wall defect unlike in the 2D case where \mathbf{n} bends and splays across the wall defect region.

However, it is important to take into account another feature of the electric field. In the 2D case values of $|\mathbf{E}^h - \mathbf{E}^l|/|\mathbf{E}^h|$ are small: 0.025 inside the wall defect layer and 0.2–0.25 in the region close to electrode edges. In the HMD case these values are about 0.1 and 0.6–0.7, respectively. The simplest way to take this fact into account is to approximate the electric potential $\Phi(\mathbf{r})$ for any voltage by

$$\Phi = \alpha \Phi^h + (1 - \alpha) \Phi^l, \quad (10)$$

where, in the simplest approximation, α is a parameter (α does not depend on \mathbf{r}). It is clear that Φ satisfies the boundary conditions of the electrodes and when $|z| \rightarrow \infty$. After substituting Eq. (10) into the free energy F , one can minimize F by choosing α as a solution to the equation $\partial_{\alpha} F = 0$. Using Eqs. (5) and (6) for $\Phi^{h,l}$, noticing that $\Phi^h - \Phi^l = 0$ on the electrodes and $\epsilon_{||} \partial_z \Phi^{h,l} = \epsilon_g \partial_z \Phi^{h,l}$ on the rest of the LC-glass interface, it is possible to exclude integrals over the glass substrates and find $\alpha = B/A$, where

$$B = \int d\rho \int_{-d/2}^{d/2} dz [\mathbf{n} \cdot \mathbf{E}^l (\mathbf{n} \cdot \mathbf{E}^l - \mathbf{n} \cdot \mathbf{E}^h) - E_z^l (E_z^l - E_z^h)],$$

$$A = B + \int d\rho \int_{-d/2}^{d/2} dz [\mathbf{E}^h (\mathbf{E}^l - \mathbf{E}^h) - \mathbf{n} \cdot \mathbf{E}^h (\mathbf{n} \cdot \mathbf{E}^l - \mathbf{n} \cdot \mathbf{E}^h)].$$

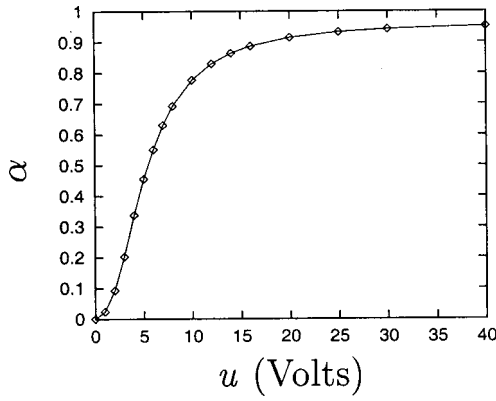
When $u \rightarrow 0$,

$$\mathbf{n} \cdot \mathbf{E} \rightarrow E_z, \quad B \rightarrow 0 \quad \text{and} \quad \alpha \rightarrow 0.$$

On the other hand, if $u \rightarrow \infty$,

$$\mathbf{n} \cdot \mathbf{E} \rightarrow E^h, \quad \mathbf{n} \cdot \mathbf{E}^h (\mathbf{n} \cdot \mathbf{E}^l - \mathbf{n} \cdot \mathbf{E}^h) \rightarrow E^h (\mathbf{E}^l - \mathbf{E}^h),$$

$A \rightarrow B$ and $\alpha \rightarrow 1$. Figures 5 and 6 display the voltage dependence of α and the v dependence of E_u , respectively; $u = \infty$ corresponds to $\mathbf{E} = \mathbf{E}^h$.

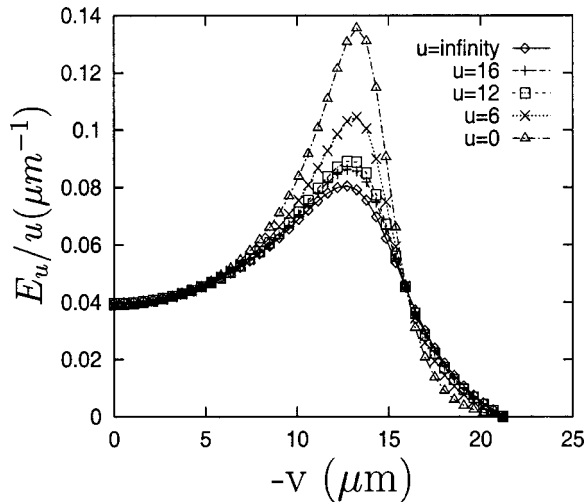
FIG. 5. Voltage dependence of α .

B. Boundary conditions for the director

Let us consider now the choice of boundary conditions for Eq. (4). Because of strong homeotropic anchoring at both substrates, $\mathbf{n} = \hat{z}$ at $z = \pm d/2$. The choice of boundary conditions along the UZ or VZ planes is not obvious. One can choose, of course, a larger volume for the director description, for example, a rectangular prism with the rectangle ABB_1A_1 of Fig. 2 as its horizontal cross section, and then use mirror symmetry to derive appropriate conditions for \mathbf{n} along the vertical planes at $x = \pm L/2$ and $y = \pm L/2$. However, this would decrease the speed of the calculation drastically (more than 10 times). To find \mathbf{n} in the smallest possible region of the HMD cell (the triangle prism), it is convenient to describe its symmetries as follows. First of all, the symmetry of the electric field can be represented in the following way:

$$\begin{aligned} \mathbf{E}(\mathbf{r}') &= R_\pi^u \mathbf{E}(\mathbf{r}), \quad \mathbf{r}' = R_\pi^u \mathbf{r}, \\ \mathbf{E}(\mathbf{r}'') &= -R_\pi^v \mathbf{E}(\mathbf{r}), \quad \mathbf{r}'' = R_\pi^v \mathbf{r}, \end{aligned} \quad (11)$$

where \mathbf{r} is an arbitrary point and R_π^α is a rotation by π about the α axis: $\alpha = u$ or v means a rotation around the U or V axis of the UVZ coordinate system produced by rotating the

FIG. 6. Shapes of $E(u=0, v, z=0)$ at different voltages u for the HMD cell; $u = \text{infinity}$ corresponds to E_u^h , and $u = 0$ corresponds to E_u^l .

XYZ system 45° around the Z axis counterclockwise (see Fig. 2). The corresponding symmetry relations for \mathbf{n} are

$$\begin{aligned} \mathbf{n}(\mathbf{r}') &= \pm R_\pi^u \mathbf{n}(\mathbf{r}), \quad \mathbf{r}' = R_\pi^u \mathbf{r}, \\ \mathbf{n}(\mathbf{r}'') &= -\pm R_\pi^v \mathbf{n}(\mathbf{r}), \quad \mathbf{r}'' = R_\pi^v \mathbf{r}, \end{aligned} \quad (12)$$

and they differ from Eqs. (11) due to uncertainty in the signs, because of $\mathbf{n} \rightarrow -\mathbf{n}$ equivalence. To take into account all those possibilities, a tensor or Q representation for the Frank free energy density,^{14–16} $f = f_d + f_e$, inside the LC cell with

$$\begin{aligned} f_d &= \frac{1}{12} (K_3 - K_1 + 3K_2) s_0^{-2} G_1^{(2)} + \frac{1}{2} (K_1 - K_2) s_0^{-2} G_2^{(2)} \\ &\quad + \frac{1}{4} (K_3 - K_1) s_0^{-3} G_6^{(3)}, \end{aligned} \quad (13)$$

$$f_e = -\frac{\epsilon_a}{8\pi s_0} E_i E_k Q_{ik} - \frac{\epsilon_\perp}{8\pi} E^2, \quad (14)$$

may be used. Here $G_1^{(2)} = Q_{ik,l} Q_{ik,l}$, $G_2^{(2)} = Q_{ik,k} Q_{il,l}$, $G_6^{(3)} = Q_{ik} Q_{lm,i} Q_{lm,k}$, $Q_{ik,l} = \partial_{x_l} Q_{ik}$ and

$$Q_{ik} \equiv Q_{ik}^{\text{Frank}} = s_0 (n_i n_k - \frac{1}{3} \delta_{ik}). \quad (15)$$

Here s_0 is a scalar order parameter which is assumed to be spatially constant but to vary with the temperature in the nematic phase.¹⁷ In this representation, the boundary conditions for Q_{ik} are completely determined. Along the UZ plane

$$\begin{aligned} Q_{ik}(\mathbf{r}') &= R_\pi^u Q_{ik}(\mathbf{r}), \quad \text{if } ik = uu, vv, vz, zz, \\ Q_{ik}(\mathbf{r}') &= -R_\pi^u Q_{ik}(\mathbf{r}), \quad \text{for } ik = uv, uz, \end{aligned} \quad (16)$$

and along the VZ plane

$$\begin{aligned} Q_{ik}(\mathbf{r}'') &= R_\pi^v Q_{ik}(\mathbf{r}), \quad \text{for } ik = uu, uz, vv, zz, \\ Q_{ik}(\mathbf{r}'') &= -R_\pi^v Q_{ik}(\mathbf{r}), \quad \text{for } ik = uv, vz. \end{aligned} \quad (17)$$

The same Q representation of the Frank free energy can be applied, of course, to the 2D cell which combines the concept of IPS with VA (see Fig. 1). The symmetry for the electric field and director for that cell may be described as follows:

$$\begin{aligned} \mathbf{E}(-x, z) &= -R_\pi^z \mathbf{E}(x, z), \\ \mathbf{n}(-x, z) &= \pm R_\pi^z \mathbf{n}(x, z), \end{aligned} \quad (18)$$

where R_π^z is the rotation by π around the z axis. Again, using the tensor representation, Eqs. (13)–(15), the boundary conditions for $Q_{ik}(x, z)$ along the $x=0$ line can be established as

$$Q_{ii}(-x, z) = Q_{ii}(x, z) \quad Q_{xz}(-x, z) = -Q_{xz}(x, z), \quad (19)$$

where $ii = xx$ or zz .

Application of the Q representation to the HMD model with the boundary conditions, Eqs. (16)–(17), produces director configurations with wall defects at least for $u < 30$ V, if an initial director distribution along the UZ plane does not deviate significantly from homeotropic. As our calculations show, in all such situations the resulting director and electric field distributions coincide with the corresponding distributions which can be found if one uses the more common vector representation, Eqs. (1)–(3), and the following boundary conditions for the director:

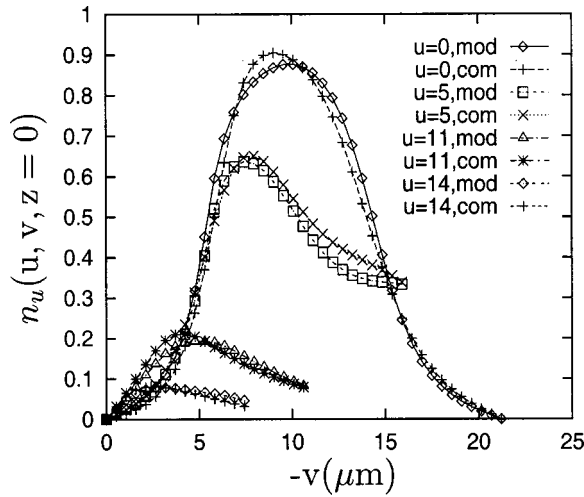


FIG. 7. $n_u(u, v, z=0)$ in the HMD cell at 7 V, calculated by the model and direct computer calculation for different values of the u coordinate (in μm).

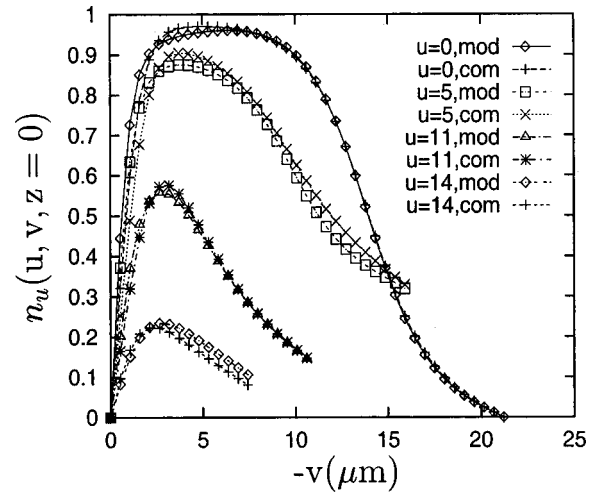


FIG. 8. $n_u(u, v, z=0)$ in the HMD cell at 11 V calculated by the model and direct computer calculation for different values of the u coordinate (in μm).

$$\begin{aligned} \mathbf{n}(\mathbf{r}') &= -R_{\pi}^u \mathbf{n}(\mathbf{r}), \quad \mathbf{r}' = R_{\pi}^u \mathbf{r}, \\ \mathbf{n}(\mathbf{r}'') &= -R_{\pi}^v \mathbf{n}(\mathbf{r}), \quad \mathbf{r}'' = R_{\pi}^v \mathbf{r}, \end{aligned} \quad (20)$$

along the UZ and VZ planes. Thus, for the voltage range most relevant for display applications, one can use the simpler and about 1.7 times faster vector representation for director calculation inside the triangular prism volume and use boundary conditions, Eqs. (20).

Exactly the same situation occurs for the 2D model. Application of the tensor representation with boundary conditions, Eqs. (19), along the z axis shows that the resulting director distributions correspond to a wall defect structure, if an initial director distribution deviates not very far from homeotropic along the $x=0$ line. In such a situation, again, the vector representation (or even θ representation, when one chooses $\mathbf{n} = \hat{x} \sin \theta - \hat{z} \cos \theta$) with the boundary condition

$$\mathbf{n}(-x, z) = R_{\pi}^z \mathbf{n}(x, z) \quad (21)$$

along the z axis may be applied, with the same results.^{4,5}

However, in both HMD and 2D cases, in principle, an alternative director configuration with $\pm 1/2$ disclination lines is possible. Using the 2D cell as an example, LC alignment and the corresponding free energy for the director configuration with disclination lines will be calculated and analyzed in detail in Sec. II C.

C. Results of the director calculations for the HMD cell

The results of the director calculation for the HMD cell are illustrated in Figs. 7–9. We have used the set of experimental cell parameters from Ref. 6. To compare this model with other methods of director calculation, the usual relaxation method for computing the director and electric field was also developed for this 3D LC cell. Figures 7–9 show $n_u(u, v, z=0)$ as a function of v for different values of the u coordinate and different voltages. For all these figures we calculated director components in two different ways: our model (taking into account the corrections described above) and direct computer calculation (relaxation method). The fig-

ures show good agreement between the model and direct computer calculation. The difference between the two results is usually within 3%–4% for all coordinates.

It is clear that the model must be faster than direct computer calculation for the following reason. As follows from the solutions $\mathbf{E}^{h,l}$ outside the LC cell,⁷ the decay of the largest (lowest) harmonics of the electric field is determined by a factor $\exp(-\pi|z|/2L)$. Because $d/L < 0.2$, it needs about L/d more mesh points in the z direction outside the cell than inside it, which increases the calculation time significantly.¹⁸ However, the gain in calculation speed M (how much faster the model is compared to direct computer calculation) depends on several factors. It depends on the dimensionality of \mathbf{n} and the type of director representation (tensor, vector or θ representation). Our calculation shows that M depends also on the method of calculation applied during simulations (for example, the method of simultaneous substitutions or the method of successive substitutions¹⁸).

In the case of the 2D model where \mathbf{n} lies in one plane, θ representation was used for both the model and direct com-

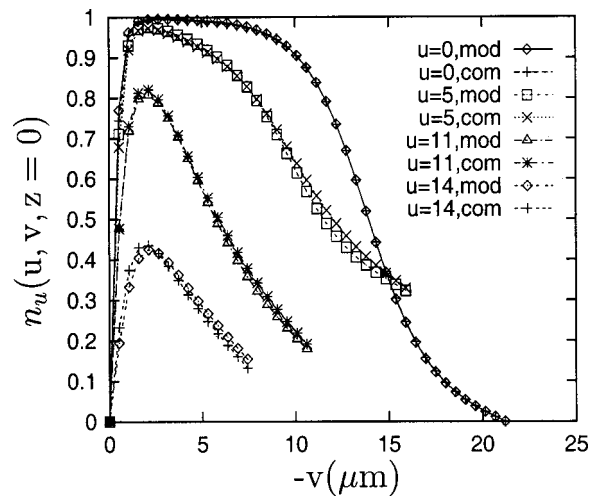


FIG. 9. $n_u(u, v, z=0)$ in the HMD cell at 16 V calculated by the model and direct computer calculation for different values of the u coordinate (in μm).

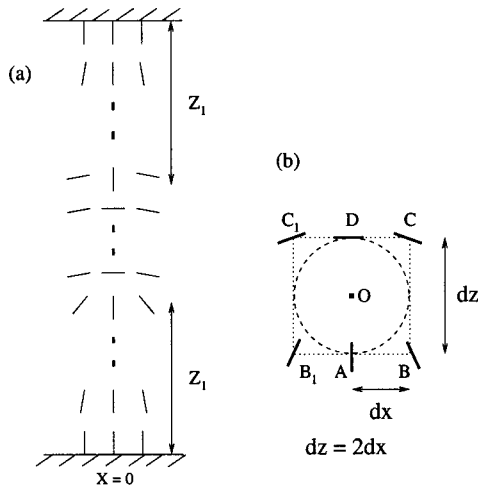


FIG. 10. (a) Director pattern in the region along the line $x=0$ in the case of $\pm 1/2$ disclination lines; (b) schematic distribution of \mathbf{n} in the xz plane in the vicinity of the $1/2$ defect line with its center at point O .

puter calculation. In this situation M is about 30–50 (M is larger for higher voltages) when the method of simultaneous substitutions is applied. Use of this method is appropriate to investigate the real (rotational) dynamics of \mathbf{n} toward the equilibrium configuration. However, calculations show that if one switches to the faster method of successive substitutions with an appropriate choice¹⁸ of the overrelaxation constant, ω (simply to find the final director distribution), direct computer calculation becomes about two times faster than simultaneous substitution. However the model improves even more and M is in the range of 130–300 (in this case M is smaller for higher u).

In the case of the HMD cell in the vector representation and using the method of simultaneous substitutions, the model gives $M \sim 25$ –40. After switching to the method of successive substitution with a proper ω , direct computer calculation becomes four to six times faster, a larger increase in speed than in the 2D case. But the model increases its calculational speed about 8–12 times, leading to $M \sim 60$ –80 for all voltages (M is slightly higher for higher u unlike in the 2D case).

III. DETERMINING LC ALIGNMENT IN A CELL WITH $\pm 1/2$ DISCLINATION LINES

An interesting and important example of application of the model is to calculate the LC alignment for a possible configuration with two $\pm 1/2$ disclination lines and its free energy F^{lines} using the 2D cell in Refs. 1–5 as an example. Figure 10(a) shows schematically the director distribution in the region along the $x=0$ plane with disclination lines that are perpendicular to the xz plane at points $z=z_1$ and $z=d-z_1$ with distance z_1 to be found and Fig. 10(b) illustrates the director pattern in the vicinity of the $+1/2$ line defect. Frank theory (either in vector or in tensor representation) cannot properly describe the director configuration inside the defect’s core region. In particular, the elastic Frank free energy diverges¹¹ if one chooses a finer mesh.

To calculate the LC alignment and F^{lines} properly, Landau–de Gennes theory with free energy density,

$$f_L = \frac{1}{2}L_1G_1^{(2)} + \frac{1}{2}L_2G_2^{(2)} + F_b(\mathbf{Q}) - F_b(\mathbf{Q}_F) - CE_iE_kQ_{ik}, \tag{22}$$

may be used inside region $ABCDC_1B_1$ in Fig. 10(b). Here $\mathbf{Q} \equiv Q_{ik}$ is a symmetric and traceless tensor order parameter, $G_1^{(2)}$ and $G_2^{(2)}$ are determined by the expressions following Eq. (13), and

$$F_b(\mathbf{Q}) = \frac{1}{2}\alpha \text{Tr} \mathbf{Q}^2 - \beta \text{Tr} \mathbf{Q}^3 + \gamma (\text{Tr} \mathbf{Q}^2)^2. \tag{23}$$

In Eqs. (22) and (23) $\alpha = a(T - T^*)$, $a, \beta, \gamma, L_1, L_2$ and C are constants and T^* is the lowest temperature to which one could supercool the isotropic phase. Typical experimental values of a, β, γ and T^* are shown in Refs. 19–21. Outside the defect core \mathbf{Q} must coincide with the uniaxial Frank form, Eq. (15), which means that $F(\mathbf{Q}) - F(\mathbf{Q}_F)$ disappears far from the core region. The nematic scalar order parameter far from the defect core, s_0 , can be found from the equation $\partial_{s_0} F_b(\mathbf{Q}_F) = 0$. The result is

$$s_0 = \frac{3\beta}{16\gamma} \left[1 + \left(1 - \frac{32\alpha\gamma}{3\beta^2} \right)^{1/2} \right]. \tag{24}$$

As is known, this form of Landau–de Gennes free energy density leads to $K_1 = K_3 = (2L_1 + L_2)s_0^2$, and we approximated these values by $(K_1 + K_3)/2$ with experimental values⁶ of K_1 and K_3 during calculation of the LC alignment inside the core. Comparison of Eqs. (13), (14) and (22) shows that in such an approximation L_1, L_2 and C may be chosen as $L_1 = K_2/(2s_0^2)$, $L_2 = (K_1 - K_2)/s_0^2$ and $C = \epsilon_a/(8\pi s_0)$.

Outside the defect core the Frank theory is correct. Moreover, because the director configuration with disclination lines is more likely to occur at high voltages for which our model is especially accurate,^{4,5} the model approach can be used to calculate the director configuration outside the defect core.

To create the resulting director distribution shown in Fig. 10, a particular initial director distribution must be chosen for the 2D cell under consideration. A key feature of the initial alignment is that the angle $\phi_{\text{init}}(0, z)$ between \mathbf{n} and \hat{z} along the $x=0$ line must be nonzero, namely, $\phi_{\text{init}}(0, z) \geq \phi^* \approx \pi/4$ when $z_1 \leq z \leq d - z_1$, and $\phi_{\text{init}}(0, z) < \phi^*$ outside this interval [$\phi_{\text{init}}(0, 0) = \phi_{\text{init}}(0, d) = 0$ for this cell].

Landau–de Gennes theory was applied in Ref. 22 in the vicinity of the nematic–isotropic transition, when $|T - T^*| \sim 1$ K. The important result that was found is that the core is biaxial²³ and does not consist of isotropic fluid, as was previously assumed.²⁴ This result was also confirmed by Monte Carlo simulation,²⁵ where molecules were represented as hard spherocylinders with aspect ratios less than or equal to 8. However, the description of LC alignment in Ref. 22 was given for the case of zero external field, and, thus, did not consider the LC alignment outside the defect’s core. The purpose of the present investigation is to provide a description of LC alignment throughout the whole cell (using Frank theory outside the core), and properly estimate F^{lines} for characteristic temperatures T of LC display applications, when $T - T^* < -10$ K. First of all, it is convenient to rewrite f_L in dimensionless variables, measuring space coordinates in units of $(L_1\gamma/\beta^2)^{1/2}$ and F_L in units of β^2/γ . The free energy density will have the same form as Eq. (22) but with

the following substitutions: $L_1 \rightarrow 1$, $L_2 \rightarrow C_2 = 2(K_1 - K_2)/K_2$, $\alpha \rightarrow \hat{\alpha} = \alpha\gamma/\beta^2$, $\beta \rightarrow \hat{\beta} = \gamma/\beta$, $\gamma \rightarrow \hat{\gamma} = \beta^2$, and $C \rightarrow \hat{C} = \epsilon_a\gamma/(8\pi s_0\beta^2)$. Choosing Q_{xx} , Q_{xy} , Q_{xz} , Q_{yz} and Q_{zz} as independent variables, one can write the Euler–Lagrange equations in terms of those variables and then solve them numerically using the relaxation method¹⁸ and boundary conditions to provide the correct asymptotic behavior at large distance r from the core. These boundary conditions will be discussed later after we describe the asymptotic behavior of Q_{ik} . For this particular LC cell it is possible to speed up calculation of Q_{ik} by solving the Euler–Lagrange equations only on the right half $ABCD$ (see Fig. 10) of the whole defect region using the symmetry of the cell which gives us the following relations: $Q_{ii}(-dr, z) = Q_{ii}(dr, z)$, where $i = x, z$, and $Q_{xy}(-dr, z) = Q_{xy}(dr, z)$, $Q_{xz}(-dr, z) = -Q_{xz}(dr, z)$, $Q_{yz}(-dr, z) = -Q_{yz}(dr, z)$ [see also Eq. (19)]. Here dr is a mesh step inside the core region which was chosen to be the same for both x and z directions. To obtain the correct boundary conditions for solving the Euler–Lagrange equations, we assume that far from the center O of the core region, in particular, along its border of $ABCD$, Q_{ik} has its Frank form,

$$(s_0 + y)(n_i n_k - \frac{1}{3}\delta_{ik}), \tag{25}$$

where $y(\mathbf{r})$ is small with respect to s_0 and $n_{x,z}$ are close to values of $n_x = \sin(\theta/2)$, and $n_z = -\cos(\theta/2)$ in cylindrical coordinates r , and θ with the center at O . Like in Ref. 4, we represent the director \mathbf{n} for $x \geq 0$ (and outside the core) as $\mathbf{n} = \hat{x} \sin \phi - \hat{z} \cos \phi$, where ϕ is the angle between \mathbf{n} and \hat{z} .

In order to describe the asymptotic behavior of Q_{ik} , it is convenient to rewrite f_L in cylindrical coordinates in the asymptotic region, where the dimensionless coordinate r is large and Q_{ik} has its Frank form, Eq. (25). The resulting Euler–Lagrange equation for $y(\mathbf{r})$ can be written as

$$\hat{L}y - N_0^2 r y = \frac{1}{r} \left(\frac{1}{2} b \cos \theta + \delta \right) s_0. \tag{26}$$

In this equation $\hat{L}y = \hat{L}_1 y + \hat{L}_2 y$ with

$$\hat{L}_1 y \equiv (1 + b \cos \theta)(y_r + y_{rr}r) - 2b \sin \theta y_{\theta r} + \frac{1}{r}(1 - b \cos \theta)y_{\theta\theta}, \tag{27}$$

$$\hat{L}_2 y \equiv b \left(\frac{1}{r} \sin \theta y_{\theta} - \cos \theta y_r \right), \tag{28}$$

and

$$b = \frac{3C_2}{C_{12}}, \quad N_0^2 = \frac{12|\alpha| + 32\hat{\gamma}s_0^2}{C_{12}}, \quad \delta = \frac{9(1 + C_2/2)}{2C_{12}}, \tag{29}$$

where $C_{12} = 12 + 5C_2$, $y_r = \partial_r y$, $y_\theta = \partial_\theta y$, $y_{\theta r} = \partial_{\theta r}^2 y$, $y_{\theta\theta} = \partial_{\theta\theta}^2 y$ and $y_{rr} = \partial_{rr}^2 y$. A solution to Eq. (26) is given by $y = y_0 + y_1$, where y_0 is a general solution of the homogeneous equation,

$$\hat{L}y_0 - N_0^2 r y_0 = 0, \tag{30}$$

and y_1 is a particular solution of the inhomogeneous equation,

$$\hat{L}y_1 - N_0^2 r y_1 = \frac{1}{r} \left(\frac{1}{2} b \cos \theta + \delta \right) s_0. \tag{31}$$

If $b = 0$, which corresponds to the one constant approximation ($K_1 = K_2 = K_3$), the θ dependence disappears in Eqs. (26)–(31), and Eq. (30) reduces to the modified Bessel equation,

$$y_{0r} + r y_{0rr} - N_0^2 r y_0 = 0. \tag{32}$$

One of the two independent solutions of Eq. (32), $K_0(N_0 r)$ [where $K_0(z)$ is the modified Bessel function of zero order], decreases exponentially with asymptotic behavior,

$$y_0 \approx \frac{c}{\sqrt{r}} \exp(-N_0 r), \quad c = \text{const}, \tag{33}$$

at $r \rightarrow \infty$. In a more realistic situation in which $b \neq 0$, the decreasing solution of Eq. (30) picks up θ dependence, and the asymptotic form is

$$y_0(r, \theta) \approx \frac{c}{\sqrt{r}} \exp[-N(\theta)r], \quad c = \text{const}. \tag{34}$$

Substituting Eq. (34) into Eq. (30) and keeping the leading terms for large r , one comes up with the following equation for $N(\theta)$:

$$(1 + b \cos \theta)N^2 - 2b \sin \theta N N_\theta + (1 - b \cos \theta)N_\theta^2 = N_0^2, \tag{35}$$

where $N_\theta \equiv \partial_\theta N(\theta)$. The desired solution of Eq. (35) must also satisfy the following conditions: $N(\theta + 2\pi) = N(\theta)$, $N(\theta) > 0$ for all θ . The exact solution is

$$N(\theta) = N_0(p + q \cos \theta), \tag{36}$$

where $p = [(1 + b)^{1/2} - (1 - b)^{1/2}]/2$ and $q = [(1 + b)^{1/2} + (1 - b)^{1/2}]/2$. For experimental values^{3,4} $K_1 = 1.32$, $K_2 = 0.65$ and $K_3 = 1.83$ (in units of 10^{-6} dyne), $C_2 = 2.89$ and $b = 0.33 < 1$, which gives $p = 1.04$ and $q = -0.17$.

The particular solution of inhomogeneous Eq. (31) can easily be found as a series in r^{-2} : $y_1(r, \theta) = y_1^{(0)}(r, \theta) + y_1^{(1)}(r, \theta) + \dots$, where

$$y_1^{(0)} = -\frac{1}{N_0^2 r^2} \left(\frac{1}{2} b \cos \theta + \delta \right), \tag{37}$$

$$y_1^{(i)} = \frac{1}{N_0^2 r} \hat{L} y_1^{(i-1)} \propto \frac{1}{r^{2(i+1)}}, \quad i = 1, 2, \dots$$

A characteristic ratio $|y_1^{(1)}/y_1^{(0)}|$ can be approximated as $4/(N_0 r)^2$ and is relatively small for $r \geq 10$, taking into account that usually N_0 is between 1 and 2.

Our estimates and calculations show that for $r \geq 10$ the exponential (homogeneous) part y_0 of the complete solution $y = y_0 + y_1$ becomes negligible with respect to y_1 , which means that the final asymptotic behavior for large r can be approximated by $y_1 \approx y_1^{(0)}$. Taking into account the approximate form of Eq. (25) for Q_{ik} and the asymptotic behavior of Eq. (37) of $y(r, \theta)$, one can write that, at large r , $\partial_r y \approx -(2/r)y \equiv -(2/r)(s - s_0)$, or, multiplying this relation by the factor $(n_i n_k - \delta_{ik}/3)$, the following relation between Q_{ik} and its radial derivative at some $r = r_c$ can be written:

$$\partial_r Q_{ik} = -\frac{2}{r_c} \left[Q_{ik} - s_0 \left(n_i n_k - \frac{1}{3} \delta_{ik} \right) \right]. \quad (38)$$

This relation was used as the boundary condition in the course of solving the Euler–Lagrange equations inside region $ABCD$ and $r_c = r_c(\theta)$ describes the contour $ABCD$ when θ varies from 0 to π [$r_c(0)$ corresponds to A].

Let us now estimate $r_c(\pi/2) \equiv dx$, a characteristic dimension of the defect core. When y is nonzero in the vicinity of contour $ABCD$, Frank coefficients K_i acquire additional factors of order s/s_0 , where $s/s_0 = 1 + y/s_0$ in the region adjacent to the defect core. If we assume that $|y/s_0| \leq \Delta s$, a small number, it will also affect the director distribution in that adjacent region with the same order of magnitude Δs . However, our calculations show that if the director distribution along $ABCD$ changes by 0.1%–1%, the entire free energy changes only by 0.01% or less, which means that the impact of this initial director deviation also decreases away from the defect region. Taking this information into account, we choose $\Delta s = 0.001$ which gives the following estimate:

$$dx = \frac{1}{N_0} \left(\frac{\delta}{\Delta s} \right)^{1/2} \quad (39)$$

(we neglected $0.5b \cos \theta$ with respect to δ for simplicity). To estimate this size in real units, one has to multiply Eq. (39) by the scaling factor $(L_1 \gamma / \beta^2)^{1/2}$. Using Eqs. (24), (29) and (39), one finds that, for example, at $\Delta T = -40$ K, $dx = 12$, or, in unscaled units of length, 100 \AA . Thus, for the temperature range of $-70 \text{ K} \leq \Delta T \leq -30 \text{ K}$, which is typical for display applications, $dx \sim 100 \text{ \AA}$. It is worth mentioning that there is always an “inner” core (with radius of about $dx/3$) where Q_{ik} deviates significantly from its Frank form.

Because the electric correlation length ξ is more than $(0.2\text{--}0.25) \mu\text{m}$ for the most relevant voltage range of $u < 100 \text{ V}$, the length scale of varying LC alignment inside the core region is about 100 times smaller than outside it. In the other words, the characteristic (elastic) free energy density inside the core which is of order $K/(dx)^2$, is three to four orders of magnitude larger than the characteristic free energy density $K/\xi^2 \propto \epsilon_a E^2/4\pi$ created by applying electric field \mathbf{E} . This comparison shows that one can determine LC alignment inside the core region of a disclination line (described by values of Q_{ik}) independently and prior to Frank calculation of the director outside the core region. The accuracy of values of \mathbf{E} inside the core does not affect the accuracy of this calculation significantly. By minimizing the free energy, Eq. (22), with respect to Q_{ik} , using Eq. (25) and neglecting y along the border of $ABCD$, one can determine director angle θ along this border, particular by at points B and C , from

$$\theta = \arcsin(Q_{xx}/s_0 + 1/3)^{1/2}. \quad (40)$$

We found that values of ϕ at those points differ by about 1% from the values $\phi = \theta/2$ (22.5° and 67.5° at points B and C , respectively). It is worth mentioning that not taking into account Landau–de Gennes theory inside the core region, and instead using only the Frank theory everywhere inside the LC cell, would give incorrect values of the director at least in the region adjacent to the defect’s core. Our calculations show, for example, that the values of ϕ at points B and C

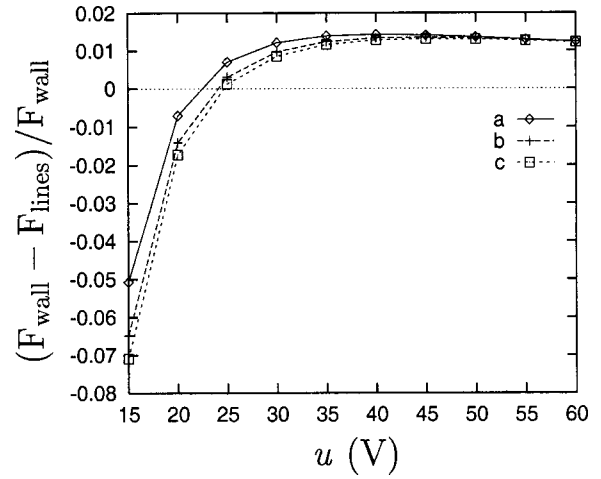


FIG. 11. Voltage dependence of $(F_{\text{wall}} - F_{\text{lines}})/F_{\text{wall}}$ for different temperature differences $\Delta T = T - T^*$. $\Delta T =$ (a) -10 ; (b) -40 ; (c) -70 K.

obtained using the Frank free energy everywhere inside the LC cell differ by 20%–30% from the Landau–de Gennes values.

Because the shape of the defect core is roughly a circle (see also Ref. 22) and due to the symmetry of this particular cell, we used mesh step $dz = 2dx$ along the region adjacent to the $x = 0$ line. A variable mesh with an increase in mesh step in the x direction was used to expedite director calculation in such a way that at a distance of $\Delta x \approx 2\xi$ from the core region in the x direction an approximate relation of $dx \approx 2dz$ is satisfied. This is reasonable, because away from the defect core \mathbf{n} varies smoothly. Inside the core region the mesh step in both the x and z directions was chosen to be $dr = dx/n$, where $n = 20$. Increasing n several times does not affect the results appreciably.

Calculations of Q_{ik} inside the core show that the behavior of its eigenvalues for $\Delta T \leq -10 \text{ K}$ is qualitatively the same as for $\Delta T \approx -1 \text{ K}$, which was shown in Ref. 22. The region where those eigenvalues and free energy density f_L differ significantly from their asymptotic values, however, shrinks when the temperature decreases in accordance with our estimate, Eq. (39), and with Eq. (24). Figure 11 illustrates a comparison between total free energies of the director configurations with a wall defect structure (F_{wall}) and with two disclination lines (F_{lines}). As is seen, the critical voltage u_* , at which this difference changes sign, is estimated to be about 24–25 V. For $\Delta T < -30 \text{ K}$ the relative difference $(F_{\text{wall}} - F_{\text{lines}})/F_{\text{wall}}$ does not depend significantly on the temperature, which is clear from Fig. 11. We have also found that the total free energy ΔF_{lines} inside the defect region depends very weakly on parameters a , β and γ of Landau–de Gennes theory. In particular, independently changing β and γ by a factor of 2 produces only about a 5% change in ΔF_{lines} , and a change in a by a factor of 2 affects ΔF_{lines} less than 1%. Because the ratio of $\Delta F_{\text{lines}}/F_{\text{lines}}$ itself is small (about 0.06 at $u = 15 \text{ V}$ and decreases inversely proportional to u^2), one can conclude that reasonable changes in a , β and γ cannot significantly alter the curves in Fig. 11, nor in particular, u_* . Because those parameters sometimes are not known exactly (unlike Frank constants), this obser-

vation makes the results of the estimation of u_* more reliable even taking into account that Landau–de Gennes theory becomes only qualitatively correct for such small temperatures.

As was mentioned earlier [see the text that follows Eq. (24)], the Landau–de Gennes free energy density [Eq. (22)] leads to $K_1=K_3$, which is inconsistent with experimental observations. As was shown in Ref. 15, including the third-order term $L_3G_6^{(3)}$, where $L_3=(K_3-K_1)/4s_0^3$, in the elastic free energy removes this degeneracy and reproduces the experimentally observed T dependence of the Frank elastic constants (at least for one LC material, PAA). Including the $L_3G_6^{(3)}$ term does not qualitatively change our calculational scheme, but it does produce the following changes in Eqs. (26)–(37): $b \rightarrow b_3 = 3(C_2 + 2C_3s_0)/C_{123}$, $N_0^2 \rightarrow N_{03}^2 = (12|\alpha| + 32\hat{\gamma}s_0^2)/C_{123}$, $\delta \rightarrow \delta_3 = [(9/2)(1 + C_2/2 + C_3s_0/6) - (9/4)C_3s_0 \cos \theta]/C_{123}$, where $C_{123} = 12 + 5C_2 + 2C_3s_0$ and $C_3s_0 = (K_3 - K_1)/K_2$. The estimate for dx [Eq. (39)] keeps the same form with the change $\delta \rightarrow \delta_1 = (9/2)(1 + C_2/2 + C_3s_0/6)/C_{123}$. The solution of the Euler–Lagrange equations for Q_{ik} is qualitatively the same. These modifications, however, produce no visible changes in Fig. 11.

All calculations inside the defect core reported here (e.g., the total free energy) were made for the 2D cell.^{1–5} However, this way of determining the LC alignment in the core region can be applied to other cells with disclination lines such as a π cell¹⁰ with a 2D director. If there is no symmetry (only periodicity in one direction), like in the case of a π cell, where the pretilt angle at the substrates differs from 0 and π , one has to solve the Euler–Lagrange equations for Q_{ik} in the whole defect region of $ABCD C_1 B_1$ using the same boundary conditions along its border. In a more complicated 3D cell (like HMD mode), this method of determining the LC alignment inside a topological defect may be used with small modifications. In this case a disclination line is not, generally, a straight line (see, for example, Ref. 7). Conditions along the line, such as the electric field, may vary from point to point. However, because the core region is essentially two dimensional (space derivatives along the line can be neglected), it is possible to choose a local 2D coordinate system xz with its origin in the center of the core and the xz plane perpendicular to the disclination line at any point along the line. Then, using this coordinate system, one can determine the LC alignment inside the core and along its border with the outside Frank region [particularly at points like B and D in Fig. 10(b)] in the manner described above. Because accurate values of \mathbf{E} are not important in those calculations, the result will be the same at any other point along the disclination line; in particular, one can choose core size dx from Eq. (39). Using relation (40) as the boundary conditions for Eq. (4), it is possible to completely determine \mathbf{n} in the rest of the LC cell outside the disclination line. To localize the disclination line, it is convenient to first make 100–200 iterations of the dynamic equation in the tensor representation using only Frank free energy. After that the coordinates of a disclination line are known. Then it is possible to determine the LC alignment inside the topological defect, as has been described here. Finally, knowing the border values of \mathbf{n} , one can complete iterative solution of the

dynamic equation in the Frank region outside the defect using the director distribution obtained after 100–200 iterations as the initial distribution. Of course, it is possible to use direct computer calculation (which includes solving the equation $\nabla \cdot \mathbf{D} = 0$) to determine \mathbf{n} in the Frank region. However, it will slow down the calculational speed about 50- to 100-fold as was already mentioned.

As one can see from Fig. 11, the defect structure with disclination lines for the 2D cell^{1–5} becomes preferable for $u > 25$ V. However, as was already mentioned, this final director distribution is only possible if angle $\phi_{\text{init}}(0, z)$ of the initial director alignment is large enough. On the other hand, application of the Q representation of the Frank free energy with boundary conditions (19) shows, in agreement with experiments,³ that only the wall defect structure is realized, at least for $u \leq 60$ V, if the amplitude of ϕ_{init} along the z axis is small. A possible explanation of this result is as follows. Let us suppose that there is a fluctuation in \mathbf{n} with a characteristic size of $a_0 \equiv dx/3 \sim 50 \text{ \AA}$ and angle of deviation of $\phi \sim 0.1 < \pi/4$ from $\mathbf{n} = -\hat{z}$ along the z axis. This produces an increase in the free energy of order $K(\phi/a_0)^2$ (where K is a Frank constant), which is more than an order of magnitude larger than the electric energy density even at $u \sim 100$ V. This means that the electric force is negligible with respect to the elastic force and the latter quickly suppresses such fluctuations.

IV. CONCLUSIONS

A simplified model was constructed to describe the director and electric field configurations in a multidimensional LC cell with a twist wall defect. This result is an extension of the description of a LC cell that has a bend and splay wall defect with the director lying in one plane. The simplified model provides an alternative to the traditional method of direct computer solution of Euler–Lagrange equations for the director and electric field in analyzing the behavior of liquid crystal cells. The model is applied to describe a 3D director in a LC cell which exhibits a homeotropic to multidomainlike transition. The calculations show good agreement between the model and direct computer calculation of the director. However, the model is much faster. In the case of using the method of successive displacement with an appropriate choice of overrelaxation constant for both the model and direct computer calculation the model is about 130–300 times faster in the 2D case and 60–80 times faster in the HMD cell.

An approximate but still accurate method of treating a LC cell with $\pm 1/2$ disclination lines using Landau–de Gennes theory inside the disclination core region was developed. It was shown that deviation of the tensor order parameter from its Frank form far from the core center decreases as $1/r^2$, where r is the distance from the center, and has azimuthal dependence. A temperature dependent estimate for the size of the defect core was found. The free energy of a cell with disclination lines was calculated and compared with the corresponding value for the same cell with a wall defect structure. For typical values of parameters of Landau–de Gennes theory, the director structure with disclination lines

becomes preferable for $u > 24\text{--}25$ V. However, the role of cell symmetry may be important in that the phase transition into the energetically preferred state may not occur even for reasonably high voltages, and the system can be trapped in a metastable state.

ACKNOWLEDGMENT

This work was supported by the National Science Foundation under Science and Technology Center Grant No. ALCOM DMR89-20147.

- ¹K. H. Kim, S. B. Park, J. U. Shim, J. Chen, and J. H. Sou, Proceedings of the Fourth Nitride Display Workshops, 1997, p. 1175.
- ²S. H. Lee, H. Y. Kim, T. K. Jung, I. C. Park, Y. H. Lee, B. G. Phon, J. S. Park and H. S. Park, in Ref. 1, p. 9.
- ³W. Liu, J. Kelly, and J. Chen, Jpn. J. Appl. Phys., Part 1 **38**, 2779 (1999).
- ⁴G. Panasyuk, D. W. Allender, and J. Kelly, J. Appl. Phys. **89**, 4777 (2001).
- ⁵G. Panasyuk, D. W. Allender, and J. Kelly, SID Dig. Tech. Papers **32**, 850 (2001).
- ⁶S. H. Lee, H. Y. Kim, Y. H. Lee, I. C. Park, B. G. Rho, H. G. Galabova, and D. W. Allender, Appl. Phys. Lett. **73**, 470 (1997).
- ⁷G. Panasyuk and D. W. Allender, J. Appl. Phys. **87**, 649 (2000).
- ⁸S. H. Lee, S. L. Lee, and H. Y. Kim, Appl. Phys. Lett. **73**, 2881 (1998).
- ⁹S. H. Lee *et al.*, SID Symp. Dig. **32**, 484 (2001).
- ¹⁰H. Mori, E. C. Garland, Jr., J. Kelly, and P. Bos, Jpn. J. Appl. Phys., Part 1 **38**, 135 (1999).
- ¹¹P. G. de Gennes and J. Prost, *The Physics of Liquid Crystals* (Oxford Science, New York, 1993), see Eqs. (3.89) and (5.32).
- ¹²S. Dickmann, Ph.D. dissertation, University Karlsruhe, Karlsruhe, Germany, 1995.
- ¹³J. E. Anderson, P. J. Bos, C. Cai, and A. Lien, SID Symp. Dig. **30**, 628 (1999).
- ¹⁴S. Dickmann, J. Fisher, O. Cossalter, and D. A. Mlinski, SID 93 Symp. Dig. 638 (1993).
- ¹⁵K. Schiele and S. Trimper, Phys. Status Solidi B **118**, 267 (1983).
- ¹⁶A. Kilian and S. Hess, Liq. Cryst. **8**, 465 (1990).
- ¹⁷The number of symmetry allowed independent $G^{(2)}$ quantities is three and the number of $G^{(3)}$ terms is six. For the special case where s_0 is spatially constant and strong anchoring prevails, only three terms are independent (two $G^{(2)}$'s and one $G^{(3)}$). The analysis of Schiele and Trimper (Ref. 15) of the temperature dependence of the elastic constants indicated that the $G^{(3)}$ term should be $G_6^{(3)}$, leading to the form given in Eq. (13).
- ¹⁸G. D. Smith, *Numerical Solution of Partial Differential Equations* (Clarendon, Oxford, 1985).
- ¹⁹D. L. Stein, Phys. Rev. B **18**, 2397 (1978).
- ²⁰H. J. Coles, Mol. Cryst. Liq. Cryst. **49**, 67 (1978).
- ²¹P. Sheng, Phys. Rev. A **26**, 1610 (1982).
- ²²N. Schopohl and T. J. Sluckin, Phys. Rev. Lett. **59**, 2582 (1987).
- ²³I. F. Lyuksyutov, Sov. Phys. JETP **48**, 178 (1978).
- ²⁴C. Fan, Phys. Lett. **34A**, 335 (1971).
- ²⁵S. D. Hudson and R. G. Larson, Phys. Rev. Lett. **70**, 2916 (1993).